Biophysical Journal, Volume 98

Supporting Material

Long-lived high strength states of ICAM-1 bonds to aL b2 integrin: II. lifetimes of LFA-1 bonds under force in leukocyte signaling

Koji Kinoshita, Andrew Leung, Scott I. Simon, and Evan Evans

ON-LINE SUPPORTING MATERIAL

Long-lived high strength states of ICAM-1 bonds to β_2 integrin: II. lifetimes of LFA-1 bonds under force in leukocyte signaling

Koji Kinoshita [†,‡] , Andrew Leung [‡], Scott Simon [§] , Evan Evans [†,‡,*]

[†] Biomedical Engineering, Boston University, Boston, MA 02215
[‡] Physics and Pathology, University of British Columbia, Vancouver, BC Canada V6T 2A6
[§] Biomedical Engineering, University of California, Davis CA 95616
[*] address correspondence to: evanse@bu.edu or evans@phas.ubc.ca

Identifying and selecting neutrophils (PMNs) for probe tests of integrin bonds

We note that following dilution of fresh finger-prick blood samples by ~10^4:1, only 30-40 white blood cells remain in a 0.15 ml micro-chamber test preparation. Neglecting an occasional tiny (2-3 μm) platelet, the adjacent figure shows the two types of white cells observed in the chambers (held at right in each image). Text-book descriptions of normal blood predict that 98% of these cells in each micro-chamber preparation are PMNs plus B and T lymphocytes. Typically, we find the smaller *top-cell type* (size 6.5-6.8 μm) in about one per 5-10 observations; whereas, the larger *bottom-cell type* (size ~ 8.5-9 μm) is more numerous. Important here, only the smaller *top-cell type* forms strong attachments to a VCAM-1 probe,

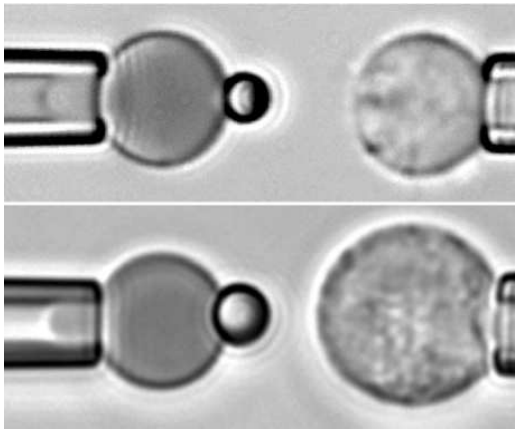

which specifically binds the β_1 integrin VLA-4. Although the *top-cell type* will bind to ICAM-1 probes, we find that formation of ICAM-1 attachments is enhanced significantly when the cells are also bound with soluble VCAM-1 (a phenomenon described as "trans-regulation" in lymphocytes, Rose et al., *J. Immunol.* 170: 5912-5918, 2003). By comparison, we do not detect VCAM-1 attachments to the *bottom-cell type* (size ~ 8.5-9 μm) beyond the level of nonspecific attachments to BSA probes, yet strong binding to ICAM-1 probes. Evident even with weak image contrast in bright field, the cell exhibits a multi-segmented nucleus surrounded by many μm-size granules which, along with cell size, characterize PMNs. At the same time, more confirmatory, its weak interaction with VCAM-1 while binding strongly to ICAM-1 distinguishes the *bottom-cell type* from the next likely candidate, but very rare (0.02:1), the eosinophil (see discussion page 2, Barthel et al., *J. Leuk. Biol.* 83, 2008). Thus, this *in situ* method of identification using VCAM-1 and ICAM-1 probes as well as size discrimination is equally valid to batch flow cytometry, yet is better suited for a population of 30 - 40 cells.

Controls for nonspecific interactions

In comparison to microsphere targets, controls for tests at surfaces of neutrophils (PMNs) yield much higher frequencies of nonspecific events and larger ranges of forces impacting statistics, even when performed with the same ~10 pN touch and 0.1 s contact. The increased number of nonspecific interactions and range of forces reflect the larger area of contact when touching a *soft* cell and the stronger hydrodynamic coupling ("suction") when retracting the cell at fast speeds (*1*). Demonstrating the enhanced nonspecifics at PMN surfaces, Figures S1A-C show controls in which the BFP was linked with an irrelevant protein (bovine serum albumin) and tested against PMNs in buffer plus 2 mM Mn^{2+} (shown as open hatched bins). Touched about a thousand times to the probe (rescaled to a common base of 10000 touches in Figs. S1), the PMNs in each control were retracted from at a fixed speed following 0.1s contact to the BFP. Typically, three retraction speeds of 2000, 10000, and 50000 nm/s were used applying linear ramps of 250, 1400, 8000 pN/s to attachments respectively in the case of nonspecific interactions.

Figure S1A-C. Nonspecific interactions of an irrelevant protein (bovine serum albumin) probe with PMNs in buffer plus 2 mM Mn^{2+}. **A-C.** Obtained from ~1000 touches in each trial, the numbers of events detected during retraction at three ramps (250, 1400, and 8000 pN/s respectively) are shown rescaled to a value per 10000 touches. The major increase in events with ramp speed shows the strong hydrodynamic coupling associated with fast retraction of soft PMNs from touch to a solid probe tip. [Note: nonspecific interactions were only counted for forces ≥ 10 pN, which accounts for the missing bins just above zero force.]

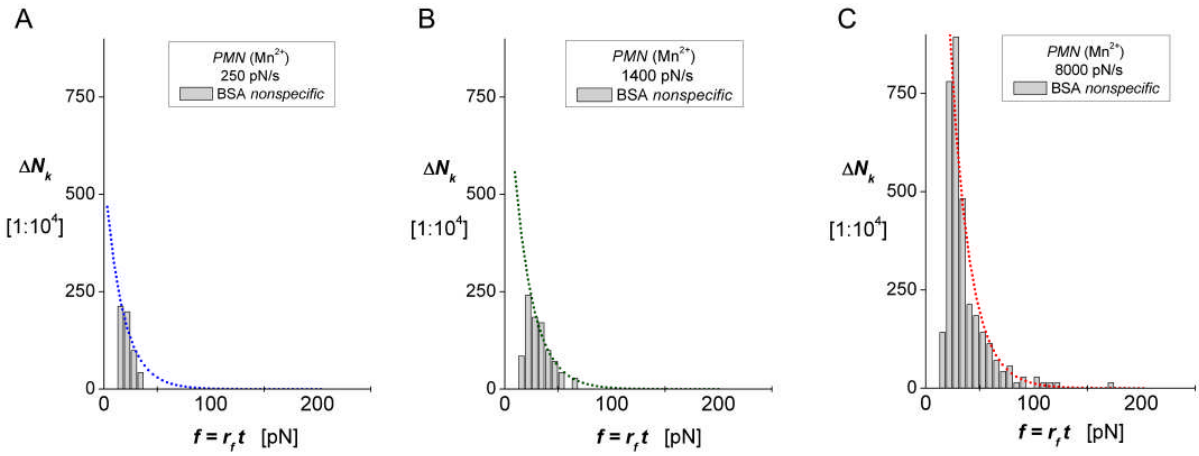

Plotted on a logarthimic scale versus force ($f = r_f t$) in Fig. S1D, the numbers of nonspecific interactions in the histograms exhibit an exponential decay with force for each ramp [i.e. $\Delta N/\Delta f \sim \exp(f/18pN)$]. Although not examined in detail, the numbers on nonspecifics are found to change with cell cortical stiffness and probe touching force. As shown in Fig. S1E, the zero-force intercepts from Fig. S1D yield a density scale $(\Delta N/\Delta f)_0$ for total number per force that increases linearly with ramp speed (i.e. velocity) as expected for hydrodynamic effects [i.e. $(\Delta N/\Delta f)_0 \approx (79 + 0.052\ r_f/pN/s)/10^4$]. By comparison, controls with rigid microspheres yield five-six fold fewer nonspecific interactions at these ramp speeds (c.f. reference *2*). Like the tests in Mn^{2+}, specific interactions between diICAM-1 and PMNs stimulated by IL-8 in 2mM Mg^{2+} were found to also drop significantly in the presence of IC487475, decreasing by ~80% as illustrated in Figs. 3D-E in the main text. By comparison, blocking both LFA-1 and MAC-1 by the anti-CD18 monoclonal R15.7 (data not shown) reduced the numbers of attachments to the levels of nonspecifics appearing in Figs. S1A-C.

Figure S1D-E. Nonspecific interactions obtained from ~1000 touches of an irrelevant protein (bovine serum albumin) probe to PMNs in buffer plus 2 mM Mn^{2+}. Plotted on a log scale in **D**, the numbers of nonspecific events are seen to diminish exponentially with force; the fits are also illustrated by the curves superposed in **A-C**. The zero-force intercepts taken from **D** are shown to increase linearly with ramp speed in **E**, i.e. $(\Delta N/\Delta f)_0 \approx (79 + 0.052\ r_f/pN/s)/10^4$. The apparent total numbers of nonspecific interactions are given by products of the zero-force intercepts and the e-fold scale of ~18 pN for exponential decay in **D**, e.g. ~ 18 $(\Delta N/\Delta f)_0$.

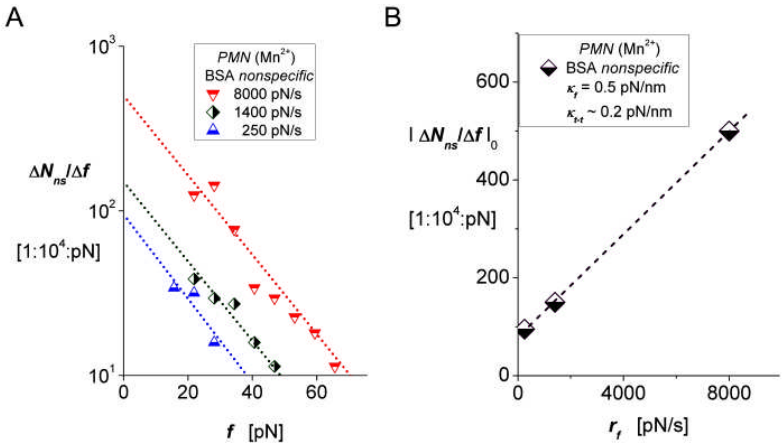

Specific ICAM-1 attachments to PMNs in Mg^{2+} *vis a vis* Mn^{2+}

When testing diICAM-1 interactions with PMNs in mM concentrations activating cations, we readily acquired distinct populations of specific attachments to PMNs in 2 mM Mn^{2+}. By comparison, very few attachments to PMNs could be detected in 2 mM Mg^{2+}. The outcome is demonstrated in Fig. S2 by the ratios of the frequencies of specific/nonspecific attachments for both 2 mM Mn^{2+} and 2 mM Mg^{2+}. As described in the main text, increasing the Mg^{2+} concentration to 5 mM produced comparable numbers of specific diICAM-1 attachments to those obtained in 2 mM Mn^{2+}. Even so, the off rates of these weak attachments were nearly ten fold faster than off rates in Mn^{2+}.

Figure S2. Ratios of frequencies for specific/nonspecific attachments from tests of a common diICAM-1 probe against PMNs in 2 mM Mn^{2+} and 2 mM Mg^{2+}.

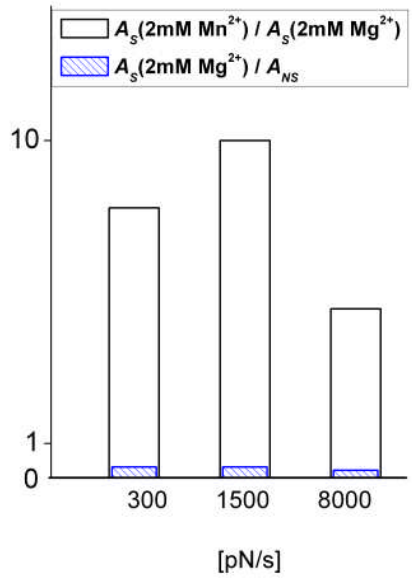

Specific inhibition of ICAM-1 interactions with LFA-1

Shown in comparison to the nonspecifics from Fig. S1, Figures S3A-C show a second set of controls between a diICAM-1 probe and PMNs in 2 mM Mn^{2+} plus 30 nM of the LFA-1 inhibitor IC487475. A member of a class of *p*-arylthio cinnamides, IC487475 is a small molecule allosteric inhibitor that binds to the I-domain allosteric site of CD11a (*3*) and has been shown to significantly interfere with PMN arrest and trans-endothelial migration (*4*).

Figure S3A-C. Interactions between a diICAM-1 probe and PMNs in 2 mM Mn^{2+} plus 30 nM IC487475 (solid magenta bins) are compared on the same scale (per 2000 touches) with nonspecifics from Figs. S1A-C (open blue patterned bins). **A-C.** Obtained from two thousand touches, the numbers of events detected during retraction are plotted versus time for three loading speeds (330, 1900, and 9000 pN/s respectively). [Note: interactions were only counted for forces ≥ 10 pN, which accounts for the missing bins just above zero force.]

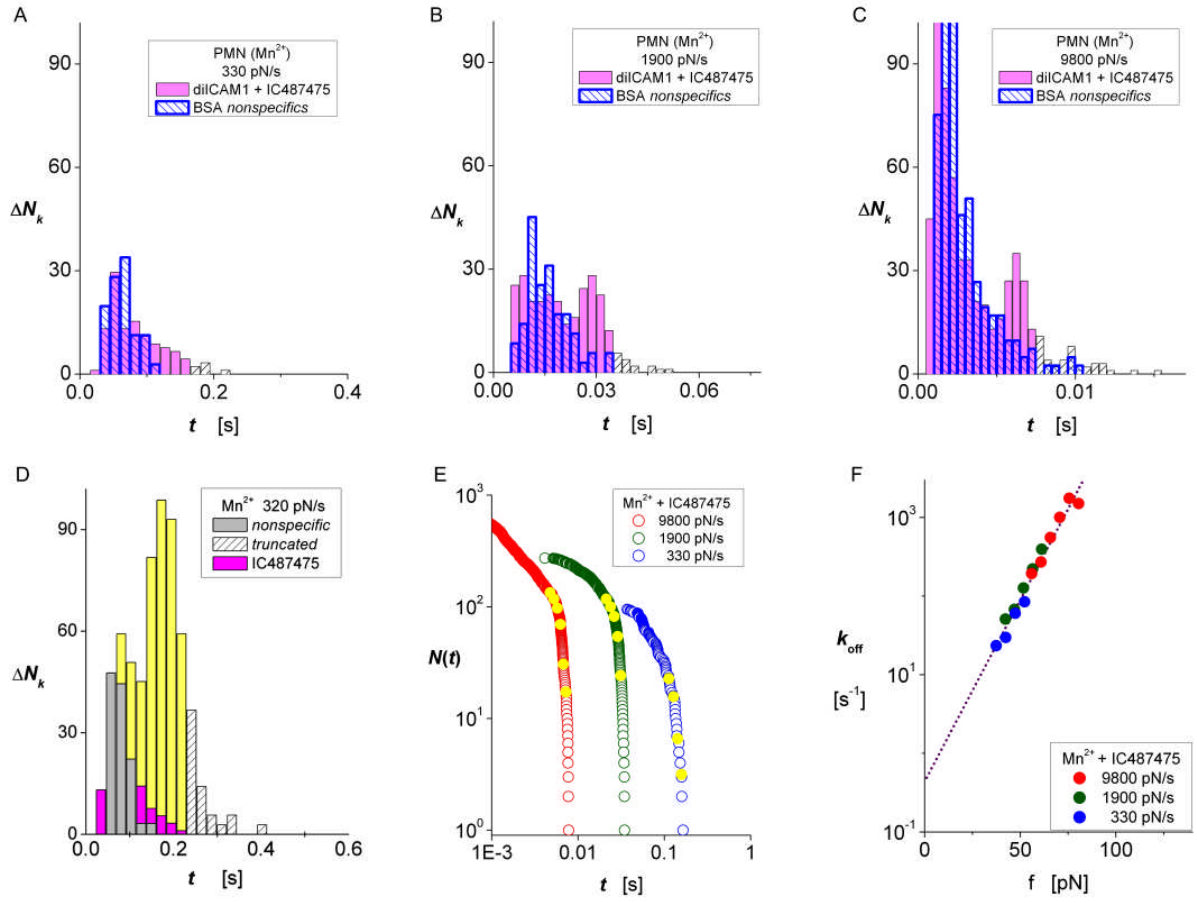

Figure S3D-F Data (yellow bins) in **D** show unbinding transitions ΔN_k obtained at a loading speed of 330 pN/s in the absence of IC487475 and rescaled per 2000 touches. Magenta bins show transitions obtained for 2000 touches in the presence of IC487475 (**A**); gray bins are the nonspecifics per 2000 touches with a BSA probe. **E.** Un-normalized probabilities $N(t)$ for attachment survival in the presence of IC487475. The unbinding transitions $\Delta N_k/\Delta t$ per time appear in **A**-**C** as magenta bins. **F.** Plotted versus force, off rates obtained from the ratios, $(\Delta N_k/\Delta t)/N(t_k)$. putatively characterize dissociation of ICAM-1 from MAC-1.

The small bulges of statistics appearing above the BSA controls in Figs. S3A-C represent 20% of the specific ICAM-1 interactions to PMNs obtained in Mn^{2+} without LFA-1 inhibition as illustrated by the overlay comparison of distributions shown in Fig. S3D. The fraction of specific ICAM-1 interactions remaining in IC487475 was 25% when PMNs were tested in Mg^{2+} plus the chemokine IL-8 (comparison to results in the absence of IC487475 appears in Fig. 3 of main text). Attributing the residual events in IC487475 to putative interactions with MAC-1, we have used the statistics of attachment lifetimes shown in Fig. S3E and histograms in S3A-C to assay the off rates. Even though the numbers of events are not large, the outcome plotted in Fig. S3F shows that the putative dissociation of ICAM-1 from MAC-1 is much faster than for ICAM-1 from LFA-1. Including the data for all three loading speeds, the linear regression in Fig. S3F yields a force-dependent off rate described by, $k_{off} \sim 0.43/s \exp(f/9.3\ pN)$. However, removing the data for 330 pN/s (blue dots) where few events exist beyond the nonspecifics, linear regression to the remaining data (green and red dots) yields a slightly faster force-dependent off rate described by, $k_{off} \sim 0.8/s \exp(f/10\ pN)$. We note that a similar force-free off rate of ~0.5 /s was recently reported from AFM tests of ICAM-1 interactions with MAC-1 expressed on CHO cells (*5*). Yet somewhat puzzling is that the mechanical strengths measured for ICAM-1 bonds to MAC-1 in the AFM tests appear larger than found for ICAM-1 bonds to LFA-1 in previous AFM tests (*6*).

ICAM-1 interactions with LFA-1 in Mn^{2+}on PMNs blocked by anti-CD11b

To confirm the dominance of LFA-1 interactions in our PMN experiments, we probed diICAM-1 interactions on PMNs in 2 mM Mn^{2+} with MAC-1 blocked by the antibody, 2LPM19fc (Dako Cytomation, Glostrop, Denmark), at two solution concentrations of 15 and 6 mg/ml (both of which gave the same result). The cells were also preincubated with the mAb prior to each micro-chamber test. Since a micro-chamber contains 0.15 ml and 30-40 cells, there were at least 10^{11} mAb/cell. Given ~5 x 10^4 MAC-1 receptors capable of binding the mAb or ICAM-1, there would be at least a 10^6 mAb/MAC-1. Thus, with great excess of mAb and a $K_D \sim 1$ nM (characteristic of blocking antibodies), we expect 99% or more of the cell surface MAC-1 to be bound by 2LPM19fc at a concentration of 15 μg/ml (0.1 μM). The same results were obtained at the lower mAb concentration of 6 μg/ml as found in functional studies using concentrations of 5 to 10 μg/ml (Lum et al., *J. Biol. Chem.* 277; 20660-20670, 2000; Hentzen et al., *Blood* 95: 911-920, 2000; Green et al., *Blood* 107: 2101-2111, 2006).

Figure S4. Interactions between a diICAM-1 probe and PMNs in 2 mM Mn^{2+} with MAC-1 blocked in a 0.1μM solution of 2LPM19fc (anti-CD11b). **A-B.** Distributions of attachment lifetimes measured at two ramp rates. **C.** Un-normalized probabilities of bond survival after truncation of Poisson multiple-attachment outliers (white patterned bins in **A**,**B**). **D.** Logarithms of off rates obtained from ratios of probability density/probability, $(\Delta N_k/\Delta t)/N(t_k)$, are plotted versus force and compared with the data (solid colored circles) taken from Fig. 2F in main text.

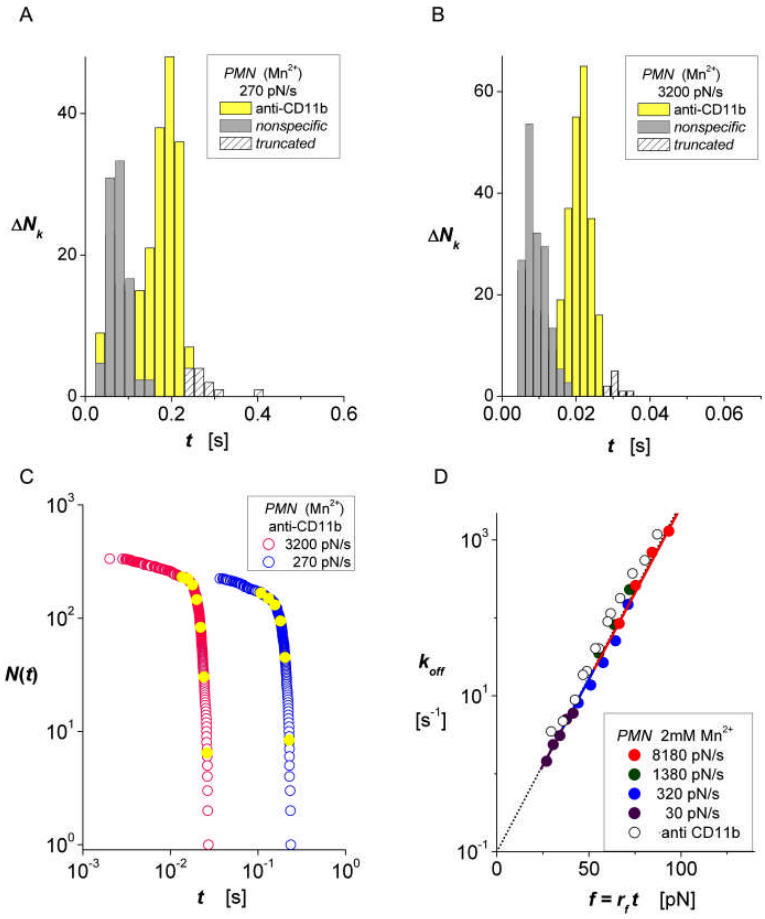

Blocking MAC-1 on PMNs diminished the numbers of specific attachments beyond the controls by about a 20% when corrected for Poisson multiples. As noted in the earlier section, the reductions in specific attachments were consistent with the residual numbers of attachments following inhibition of LFA-1 by IC487475. Most important, as shown in Fig. S4D, the off rates determined from the lifetime statistics and distributions for 2LPM19fc blocked PMNs closely match the results obtained from unblocked PMNs (taken from Fig. 2F).

Slow-hyperfast double ramp test of ICAM-1 interactions with LFA-1 on PMNs in IL-8

To test interactions with PMNs at high forces, a useful approach in many cases is to apply a sequence of slow (~200 pN/s) then extremely fast (~10000 pN/s) ramps after touch, thereby diminishing the hydrodynamic coupling under rapid retraction. Demonstrated in Fig. S5A, the piezo actuator was programmed to retract the cell after touch at a slow speed (2000 nm/s) for a period of time (~0.16s) designed to reach a pulling force of ~30 pN. The retraction speed was then immediately increased to a hyperfast speed (100000 nm/s) until the attachment failed. Resulting a slower sequence of probe deflection speeds (~450 nm/s and ~20000 nm/s) because of small PMN elasticity (~0.25 pN/nm), Figure S5A shows a sample trace for the tests of PMNs in 2 mM Mg^{2+} plus saturating concentrations of the chemokine IL-8 using a diICAM-1 probe with a spring constant of 0.5 pN/s. Subtracting out the nonspecific interactions predicted by the control, we found that a significant number of attachments failed in the slow ramp phase as

shown by the histogram in Fig. S5B. Finding a comparable population of weak attachments for all periods of exposure to IL-8, we hypothesized that the rapid failure events arose from diICAM-1 interactions with unstimulated LFA-1. Supporting this hypothesis, we show the distribution of failure times in Fig. S5B predicted by the off rates measured in 5 mM Mg^{2+} (see main text). Yet, by comparison, more than twice as many specific attachments survived at 5-10 min of exposure in IL-8 to reach large forces in the fast ramp phase, revealing a separate population of interactions. Affected negligibly by the low forces experienced in the slow ramp phase, the times measured for survival during the hyperfast ramp are plotted in Fig. S5C along with the array of single ligand statistics obtained by truncating the putative long-lived multiple attachments. The corresponding histogram of unbinding events for this population is plotted directly below in Fig. S5D. As shown in Fig. 3F of the main text, the off rates obtained from the ratios for probability density/probability, $(\Delta N_k/\Delta t)/N(t_k)$, correlate precisely with the dependence on force measured with single ramps up to ~3000 pN/s.

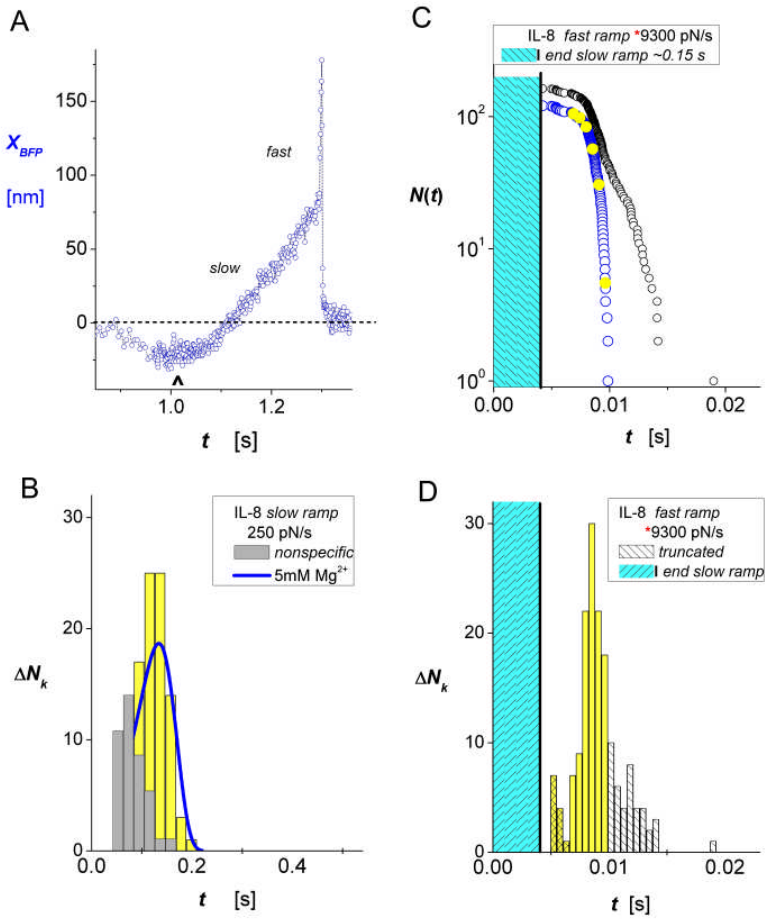

Figure S5. A. Example of BFP deflection versus time during double ramp loading of a PMN surface bond to diICAM-1 in Mg^{2+} plus IL-8. After initial contact (negative deflection marked by up arrow), the trace begins with a ~0.15s period of slow deflection at ~450 nm/s followed by 0.0044s of the fast deflection at ~20000 nm/s. With the value of 0.5 pN/m for the spring

constant, the slow/fast retraction sequence produced a double force ramp of ~225 pN/s and 10000 pN/s leading to detachment at 89 pN. **B.** Histogram of unbinding events ΔN_k measured during the slow ramp phase. Appearing behind nonspecific interactions from controls (solid gray bins), the solid yellow bins presumably reflect weak interactions with unstimulated LFA-1 in Mg^{2+}, evidence for which is the distribution (blue solid curve) predicted by the results in 5 mM Mg^{2+} (see main text, *2*). **C.** "Raw" data (open black circles) for attachment survival during the fast ramp phase along with the array $N(t_i)$ (open blue circles) of "single ligand" statistics that follow truncation of the putative multi-attachment outliers. **D.** Histogram of unbinding events ΔN_k for the fast ramp phase corresponding to the survival times plotted in **C**. Logarithms of the ratios for probability density/probability, $(\Delta N_k/\Delta t)/N(t_k)$, are plotted versus the forces at the bin center times ($f_k = r_f t_k$) in Fig. 3F of the main text. [Note: the time origins in **C,D** are defined by extrapolation of the fast ramp back to zero force.]

ICAM-1 interactions with β_2 integrin on PMNs when activated allosterically by mab 240Q

As described in the main text, we measured off rates of diICAM-1 from a high affinity state of β_2 integrin on PMNs induced by the activating monoclonal 240Q (*7*,*8*), comparing the consequences of "outside-in" signaling to the results for "inside-out" signaling in IL-8. Here we show the results from a second set of experiments using four ramps spanning a large range from 20 pN/s to 3600 pN/s, obtaining distributions with narrow peaks of specific interactions as shown by the example in Fig. S6A. Like the results for chemokine stimulation in Fig. S5D and Figs. 3D-E in the main text, the narrow peak of unbinding transitions in Fig. S6A reveals a precipitous shortening of bond lifetime under the rising force. This rapid change in lifetime is clearly evident in the arrays $N(t_i)$ (open blue circles) of events in Fig. S6B, which summarize the second experiment in 240Q. Using the statistics of bond survival and histograms obtained from the second 240Q test, we have determined the instantaneous values for off rates the bin center times t_k and show logarithms of the data plotted versus the forces ($f_k = r_f t_k$) corresponding to each ramp in Fig. S6C.

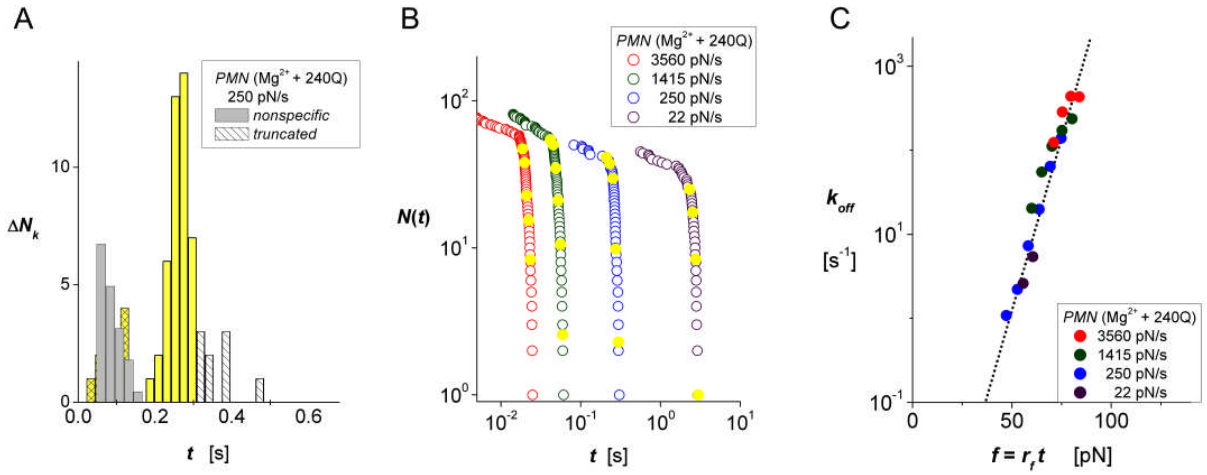

Figure S6. ICAM-1 interactions with β_2 integrin on PMNs under force when activated allosterically in mM Mg^{2+} and a saturating concentration of the monoclonal 240Q (*5*,*6*). **A.** Distribution of attachment lifetimes measured at a ramp rate of 250 pN/s. **B.** Plotted on a log-log scale, un-normalized probabilities of survival $N(t_i)$ for four ramps from 22 to 3560 pN/s (*open colored circles*) demonstrate the full range of lifetimes tested in the second 240Q experiment.

Closed yellow circles superposed on each array identify interpolation values $N(t_k)$ at centers t_k of the corresponding histogram bins. Logarithms of the ratios for probability density/probability, $(\Delta N_k/\Delta t)/N(t_k)$, are plotted versus the forces ($f_k = r_f t_k$) for each ramp in **C** and appear as open circles in Fig. 4C of the main text.

Mechanical strengths of diICAM-1 interactions with LFA-1 on the PMN surface

Because PMN and other cell interfaces are soft materials, the likelihood of rebinding to receptors after dissociation vanishes even when subjected to small forces. Consequently, ligand-integrin interactions in the circulation are formed repeatedly, loaded over a limited period of time, and failing in adhesion processes (*9*). Lacking permanent strength, the mechanical performance of the adhesive bond is best characterized by its dynamic strength, a simple measure of which is the most frequent force f^* for rupture in ramp loading r_f. Given off rates that increase exponentially under force as in Figs. 2F, 3F, and 4C, the measures of mechanical strength depend logarithmically on ramp speed (*10*), $f^* = f_\beta \ln[r_f/(k_o f_\beta)]$. Hence, the kinetic parameters in Table 1 obtained from linear regressions to the data predict how strengths of diICAM-1 attachments to LFA-1 change under different force rate conditions. As shown in Fig. S7, signaling to LFA-1 in PMNs leads to a prominent onset of strength at very low stress rates, which is absent in divalent cations alone. Moreover, the hyper-strength states demonstrated in Fig. S7 show little sensitivity to stress rate, enabling firm adhesion over a wide range of loading conditions.

Figure S7. Dynamic strengths of diICAM-1 interactions with LFA-1 on PMNs predicted by measurements of off rates versus pulling force.

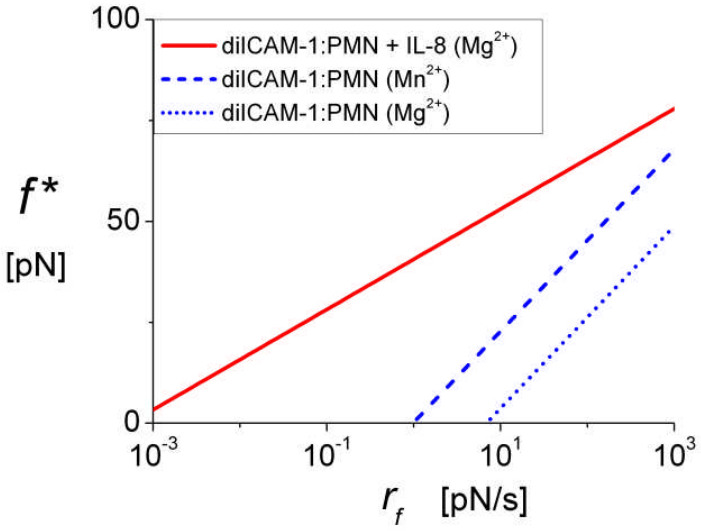

Dissociation rates of dimers under force

As described in Williams and Evans, 2002 (*11*), the kinetics of dissociation for dimers under force are impossible to predict without defining the extent of cooperativity between the two interactions and how the applied force is partitioned between each interaction. However, there are three scenarios that encompass the principal limiting regimes of detachment. The trivial scenario is that the two bonds dissociate cooperatively (i.e. at the same time) under force. Such a *cooperative* complex acts like a "single" bond and its dissociation can be characterized by a two-state process (*12*,*13*). The distinguishing feature of cooperativity is that activation energy becomes greater, resulting in a much slower rate of dissociation. By comparison, other scenarios for dimeric bonds involve random dissociation of the two interactions. In this situation, the process of dissociation involves transitions between three states, i.e. progressing from the initial dimer state (subscript label 2) via a transient monomer state (subcript label 1) to the fully dissociated state (subscript label 0), as described by the following equations:

$$\begin{aligned} dS_2(t)/dt &= - k_{2\to1}(t)\, S_2(t) + k_{2\leftarrow1}(t)\, S_1(t) \\ dS_1(t)/dt &= - [k_{1\to0}(t) + k_{2\leftarrow1}(t)]\, S_1(t) + k_{2\to1}(t)\, S_2(t) \\ dS_0(t)/dt &= k_{1\to0}(t)\, S_1(t) \end{aligned} \qquad \text{(A1)}$$

two forward rates of transition $k_{2\to1}$, $k_{1\to0}$ plus a reverse rate $k_{2\leftarrow1}$. Since release of one arm of a macromolecular ligand leads to significant separation within a dimer, we will neglect internal rebinding under force [i.e. $k_{2\leftarrow1}(t) = 0$]. Given initial conditions $S_2(0) = 1$ and $S_1(0) = S_0(0) = 0$, the probabilities for being in each state over time reduce to a set of general integral solutions,

$$\begin{aligned} S_2(t) &= \exp\left[-\int_{0\to t} k_{2\to1}(t')\, dt' \right] \\ S_1(t) &= \exp\left[-\int_{0\to t} k_{1\to0}(t')\, dt' \right] \int_{0\to t} k_{2\to1}(t') \exp\left\{ \int_{0\to t'} [k_{1\to0}(t'') - k_{2\to1}(t'')]\, dt'' \right\} dt' \\ S_0(t) &\equiv 1 - [S_2(t) + S_1(t)] \end{aligned} \qquad \text{(A2)}$$

We will use these relations to determine how internal force partitioning affects the off rates of dimeric bonds.

In probe experiments, the ratios of probability density/probability obtained from measurements of attachment lifetimes, $[p_2(t) + p_1(t)]/[S_2(t) + S_1(t)]$, provide the rate of dimer dissociation at any time, $k_{dimer}(t)$. Yet, the dissociated states emerge at a rate set by the final monomer unbinding transition which, in turn, equals the sum of probability densities for being in the dimer and monomer states over time, $[p_2(t) + p_1(t)] = k_{1\to0}(t)\, S_1(t)$. Thus, the ratio of probabilities $S_1(t)/S_2(t)$ for being in the transient monomer and dimer states determines the connection between “dimer” off rate and the rate of a “single interaction” dissociation,

$$k_{dimer}(t) = k_{1\to0}(t)\, S_1(t) / \{ S_1(t) + S_2(t) \} \qquad \text{(A3)}$$

Hence, the statistics of both states are involved in an assay for the rate of monomer dissociation. However, in most force probe experiments, we can only measure the lifetimes of dimers, which depend on the ratio of probabilities $S_1(t)/S_2(t)$ defined by Eqs. A2,

$$S_1(t)/S_2(t) = \exp\left\{ -\int_{0\to t} [k_{1\to0}(t') - k_{2\to1}(t')]\, dt' \right\} \int_{0\to t} k_{2\to1}(t') \exp\left\{ \int_{0\to t'} [k_{1\to0}(t'') - k_{2\to1}(t'')]\, dt'' \right\} dt' \qquad \text{(A4)}$$

We will use Eq. A4 to predict dimer off rates under two limiting conditions of force partitioning, thereby providing a means to evaluate the most likely internal loading condition through comparison to off rate measurements. The two extremes of internal force partitioning are labelled "zipper" and "parallel-loaded" dimers. The "zipper" dimer represents a loading sequence in which all of the force acts initially on one interaction until it dissociates then transfers the full force to the second interaction until the complex fails. The "parallel-loaded" dimer represents the other loading limit in which the force is split equally between the two interactions initially until one dissociates then doubles the force applied to the remaining interaction until the complex fails.

Beginning with the *zipper dimer*, the transition rates from dimer-to-monomer and monomer-to-detached state are identical, i.e. $k_{2\to1}(f) = k_{1\to0}(f)$, resulting in simple expressions for the ratio of probabilities at any time and the dimer off rate,

$$S_1(t)/S_2(t) = \int_{0\to t} k_{1\to0}(t')\, dt'$$
$$k_{Zdimer}(t) = k_{1\to0}(t) \int_{0\to t} k_{1\to0}(t')\, dt' / [1 + \int_{0\to t} k_{1\to0}(t')\, dt'] \quad \text{(A5)}$$

Postulating that rates for dissociation increase exponentially under force [$k_{1\to0} = k_o \exp(f/f_\beta)$] and forces follow a ramp in time [$f(t) = r_f t$], the ratio of probabilities for monomer and dimer states increases exponentially with time or force (Williams and Evans, 2002),

$$S_1(f)/S_2(f) = [\exp(f/f_\beta) - 1]/c_r \quad \text{(A6)}$$

$c_r \equiv r_f/(k_o f_\beta)$ defines the dimensionless ramp speed. Thus, off rates for a zipper dimer curve significantly downward at low forces and asymptotically approach the rate of monomer dissociation at high forces,

$$k_{Zdimer}(f) = k_o \exp(f/f_\beta)\, [\exp(f/f_\beta) - 1] / [\, c_r + \exp(f/f_\beta) - 1] \quad \text{(A7)}$$

As shown in Fig. S8A, deviation of the dimer off rates from the monomer kinetics increases progressively with faster ramps.

By comparison to zipper loading, rates can differ enormously between the dimer-monomer and monomer-detached transitions in "equally-stressed" dimers. When the two interactions dissociate randomly and the rates depend exponentially on force, the first transition will occur at the frequency, $k_{2\to1} = 2\, k_o \exp(f/2f_\beta)$, whereas the second transition increases much more rapidly with force at a frequency, $k_{1\to0} = k_o \exp(f/f_\beta)$. For forces that follow a ramp in time, the ratio of probabilities for monomer and dimer states in time again depends on the dimensionless ramp speed, $c_r \equiv r_f/(k_o f_\beta)$, and the exponential function, $g(f) \equiv \exp(f/2f_\beta)$,

$$S_1(f)/S_2(f) = (4/c_r) \exp\{ -[g(f) - 2]^2/c_r \} \int_{1\to g(f)} dy \exp[(y - 2)^2/c_r] \quad \text{(A8)}$$

Using the transformation, $w \equiv [\exp(f/2f_\beta) - 2]/c_r^{1/2}$, we reduce Eq. A8 to an expression involving Dawson's integral [$D(w) \equiv \exp(-w^2) \int_{0\to w} \exp(y^2)\, dy$],

$$S_1(f)/S_2(f) = 4\, [D(w) + \exp(-w^2 + 1/c_r)\, D(1/c_r^{1/2})]/c_r^{1/2}$$

Although seeming formidable, well-known power series and asymptotic expansions exist for Dawson's integral (*14*), which predict two distinct regimes for the ratio of probabilities $S_1(t)/S_2(t)$

and the corresponding expressions for dimer off rates. For $w < 1$, the integral increases as an alternating series, $D(w) \approx w\,[1 - (2/3)\,w^2 + (4/15)\,w^4 - (8/105)\,w^6 + \ldots]$, approaching ~0.5 at $w \sim 1$. Then, for $w > 1$, the integral diminishes rapidly in close approximation to the lead term in an asymptotic expansion, $D(w) \approx 1/(2w)$. The cross over from one regime to the next occurs at a force $f_{\otimes}$ set by $w \sim 1$ and, thereby, the dimensionless ramp speed, i.e. $f_{\otimes} = 2\,f_{\beta} \ln(2 + c_r^{1/2})$.

In the low force regime defined by, $f < f_{\otimes}$, the time needed for final transition from the monomer-to-dissociated state is an important retarding factor in dimer dissociation along with the initial dissociation from the dimer-to-monomer state. The consequence is to create a threshold-like behavior for off rates that depends strongly on ramp speed as shown in Fig. S8B. Crudely defining $D(w) \sim w/2$ in the low force regime, we obtain a good approximation to the precise numerical computations for off rates plotted in Fig. S8B, i.e.

$$k_{PLdimer}(f) \approx k_o \exp(f/f_{\beta})\,[\exp(f/2f_{\beta}) - 1] \,/\, [\exp(f/2f_{\beta}) - 1 + c_r/2] \qquad \text{(A9)}$$

By comparison, the situation is much simpler in the high force regime, $f > f_{\otimes}$. Here, off rates are completely dominated by the time needed for the initial dimer-to-monomer transition and thus follow a single exponential that depends only on force level,

$$k_{PLdimer}(f) \approx 2k_o \exp(f/2f_{\beta}) \qquad \text{(A10)}$$

Hence, when the two dimer interactions start out equally stressed, dimers essentially require a force greater than $f_{\otimes} = 2\,f_{\beta} \ln(2 + c_r^{1/2})$ to dissociate frequently. Yet, at the same time, parallel-loaded dimers dissociate much slower than monomers (cf. Fig. S8B).

Even when kinetics of the monomer interactions depend only on applied force, the three-state kinetics involved in dimer dissociation depend explicitly on time as well as force, which is demonstrated by the explicit dependences on ramp speed in Eqs. A6-9 and Figs. S8A-B. Thus, the predictions for dimer off rates in experiments change with different modes of force application. For example, consider a rapid step to a constant force level (called a “force clamp”). The statistics of dimer lifetimes, $\sim[S_1(t) + S_2(t)]$, do not decay as a single exponential in time with a constant rate but rather are expressed by,

$$S_2(t) + S_1(t) = \exp(-k_{1\to0}\,t)\,[1 + k_{1\to0}\,t]$$

for a zipper dimer and,

$$S_2(t) + S_1(t) = [\,k_{1\to0} \exp(-k_{2\to1}\,t) - k_{2\to1} \exp(-k_{1\to0}\,t)\,] \,/ (k_{1\to0} - k_{2\to1})$$

for a parallel-loaded dimer (noting the obvious special case when $k_{1\to0} = k_{2\to1}$). As with force ramps, the frequencies for both types of dimer dissociation are zero at zero force and then increase at long times to approach either the rate for monomer-to-detached state transition in the case of a zipper dimer or the rate for dimer-to-monomer transition in the case of a parallel-loaded dimer. Thus, we can only determine unique relations between force level and dimer kinetics at constant force from the average lifetimes, $\langle t_{dimer} \rangle = \int_{0\to\infty} [S_2(t) + S_1(t)]\,dt$. Again idealizing rates of transitions as exponential functions of force, we show the effective off rates for zipper and parallel-loaded dimers versus force in Fig. S8C as determined by their reciprocal average lifetimes, i.e. $1/\langle t_{Zdimer} \rangle = k_{1\to0}/2$ and $1/\langle t_{PLdimer} \rangle = k_{1\to0}\,k_{2\to0}/(k_{1\to0} + k_{2\to0})$. Although exhibiting similar limits at large forces, the functional forms for off rates under ramps of force in Eqs. A7 and A9 differ significantly from the reciprocal average lifetimes under constant forces, again as a consequence of the differences in explicit dependence on time.

Figure S8. Off rate kinetics for dimers under pulling forces. **A.** Off rates for zipper dimers versus the instantaneous level of force, $f \equiv r_f t / f_\beta$, set by the dimensionless ramp speed, $c_r \equiv r_f / (k_o f_\beta)$, based on the exponential dependence of monomer off rate on force (dotted line). **B.** Off rates for parallel-loaded dimers versus the instantaneous level of force, again defined by the dimensionless ramp speed and parameters characterizing the exponential dependence of monomer off rate on force (dotted line). Here, two dynamical regimes (corresponding colored dashed and solid curves) are found for the off rates above/below the crossover force set by ramp speed, i.e. $f_\otimes = 2 f_\beta \ln(2 + c_r^{1/2})$. For comparison, the reciprocal mean lifetimes for the dimer models held at constant force are plotted in **C**.

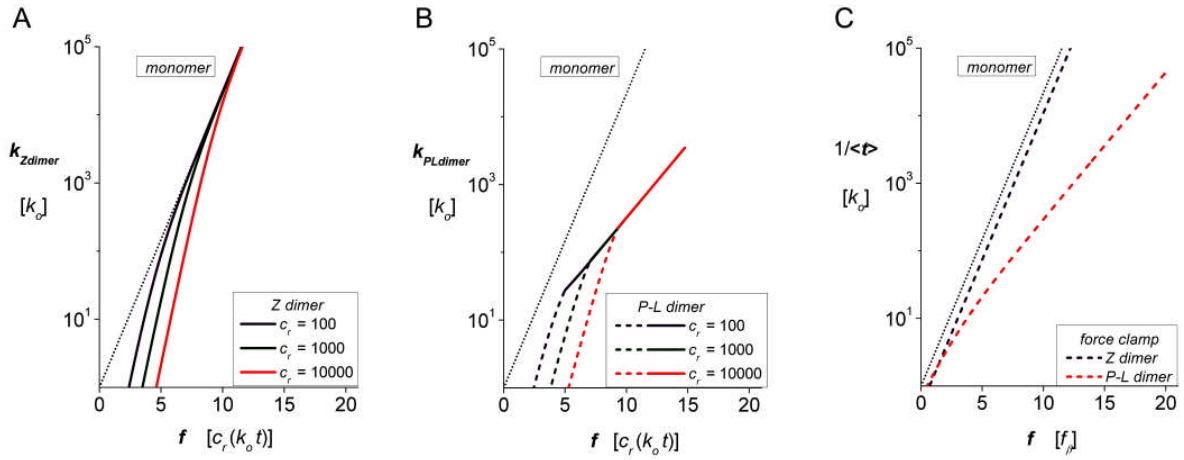

REFERENCES

1. Evans, E., Heinrich, V., Leung, A., and K. Kinoshita. 2005. Nano-to-micro scale dynamics of P-selectin detachment from leukocyte interfaces: I. membrane separation from the cytoskeleton *Biophys. J.* 88: 2288-2298.

2. Evans, E., K. Kinoshita, S.I. Simon, and A. Leung. 2009. Long-lived high strength states of ICAM-1 bonds to β_2 integrin: I. lifetimes of bonds to recombinant $\alpha_L \beta_2$ under force. *Biophys. J.* (accepted with minor revisions)

3. Winn, M., E.B. Reilly, G. Liu, J.R. Huth, H-S. Jae, J. Freeman, Z. Pei, Z. Xin, J. Lynch, J. Kester, T.W. von Geldern, S. Leitza, P. De Vries, R. Dickinson, D. Mussatto and G.F. Okasinski. 2001. Discovery of novel p-arylthio cinnamides as antagonists of leukocyte function-associated antigen-1/intercellular adhesion molecule-1 interaction, 4: structure-activity relationship of substituents on the benzene ring of the cinnamide. *J. Med Chem.* 44: 4393-4403.

4. Green, C.E., U.Y. Ulrich, M.R. Sarantos, A. F. H. Lum, D. E. Staunton and S.I. Simon. 2006. Dynamic shifts in LFA-1 affinity regulate neutrophil rolling, arrest, and transmigration on inflamed endothelium. *Blood* 107:2101-2111.

5. Yang, H., J. Yu, G. Fu, X. Shi, L. Xiao, Y. Chen, X. Fang, and C. He. 2007. Interactions between single molecules of Mac-1 and ICAM-1 in living cells: An atomic force microscopy study. *Exp. Cell Res.* 313: 3497-3504.

6. Wojcikiewicz, E.P., M.H. Abdulreda, X. Zhang, and V.T. Moy. 2006. Force spectroscopy of LFA-1 and its ligands ICAM-1 and ICAM-2. *Biomacromolecules* 7: 3188-3195.

7. Lupher, M.L. Jr, E.A. Harris, C.R. Beals, L-M. Sui, R.C. Liddington, and D.E. Staunton. 2001. Cellular activation of Leukocyte Function-associated Antigen-1 and its affinity are regulated at the I domain allosteric site. *J. Immunol.* 167: 1431-1439.

8. Beals, C.R., A.C. Edwards, R.J. Gottschalk, T.W. Kuijpers, and D.E. Staunton. 2001. CD18 activation epitopes induced by leukocyte activation. *J. Immunol.* 167: 6113-6122.

9. Evans, E., D. Calderwood. 2007. Forces and bond dynamics in cell adhesion. *Science* 316: 1148-1153.

10. Evans, E., and K. Ritchie. 1997. Dynamic strength of molecular adhesion bonds. *Biophys. J.* 72: 1541–1555.

11. Williams, P., and E. Evans. 2002. Dynamic force spectroscopy: II. multiple bonds. In Physics of Bio-Molecules and Cells, *Les Houches: Ecoles d'Ete de Physique Theorique*, (EDP Sciences-Springer) Vol. 75, pp. 145 - 185.

12. Evans, E., and K. Ritchie. 1997. Dynamic strength of molecular adhesion bonds. *Biophys. J.* 72: 1541–1555.

13. Evans, E., K. Halvorsen, K. Kinoshita, and W.P. Wong. 2009. A new approach to analysis of single molecule force experiments. Chapter 20. In Handbook of Single-Molecule Biophysics. P. Hinterdorfer and A. van Oijen editors. Springer Science + Business Media, LLC, pp. 571-589.

14. Spanier, J. and K.B. Oldham. 1987. An Atlas of Functions. Hemisphere, Washington DC.